Surface polaritons in a negative-index metamaterial with active Raman gain

Chaohua Tan[1] and Guoxiang Huang[1,2,*]

[1]*State Key Laboratory of Precision Spectroscopy and Department of Physics, East China Normal University, Shanghai 200062, China*

[2]*ECNU-NYU Joint Physics Research Institute at NYU-Shanghai, Shanghai 200062, China*

(Received 15 October 2014; revised manuscript received 20 December 2014; published 2 February 2015)

We propose a scheme to realize stable propagation of linear and nonlinear surface polaritons (SPs) by placing a N-type four-level quantum emitters at the interface between a dielectric and a negative-index metamaterial (NIMM). We show that in linear propagation regime SPs can acquire an active Raman gain (ARG) from a pump field and a gain doublet appears in the gain spectrum of a signal field induced by the quantum interference effect from a control field. The ARG can be used not only to completely compensate the Ohmic loss in the NIMM but also to acquire a superluminal group velocity for the SPs. We also show that in the nonlinear propagation regime a huge enhancement of the Kerr nonlinearity of the SPs can be obtained. As a result, ARG-assisted $(1+1)$- and $(2+1)$-dimensional superluminal surface polaritonic solitons with extremely low generation power may be produced based on the strong confinement of the electric field at the dielectric-NIMM interface.

DOI: 10.1103/PhysRevA.91.023803 PACS number(s): 42.65.Tg, 05.45.Yv

I. INTRODUCTION

The study of surface plasmon polaritons (SPPs), i.e., propagating excitations of charge-density waves and their associated electromagnetic fields along metal-dielectric interfaces, is a main issue in nanoplasmonics [1,2]. Recently, the resonant interaction between light and quantum emitters doped at metal-dielectric interfaces has become an active research field, which involves quantum-mechanical control of SPPs at subwavelength scales and quantum optical applications including the design of active plasmonic devices [3–15].

For many optical processes based on SPPs, long-distance propagation is necessary. However, the propagation length of SPPs is severely limited by high Ohmic loss in metals, which is a main impediment for further progress towards practical nanoplasmonic devices. Compensating the Ohmic loss with a gain medium at room temperature has become an important topic in the research of nanoplasmonics [5]. Up to now, several schemes for overcoming this limit have been proposed. One scheme is to introduce two-level quantum emitters into the dielectric-metal interface [3–8,12,13]. Although the gain provided by the quantum emitters can be used to compensate the loss in the metal, restrictions still exist for increasing the SPP propagation length and obtaining high quantum efficiency [5]. Several different proposals based on doped multiple-level quantum emitters in plasmonic structures have also been suggested [14,15].

Another scheme is to introduce quantum emitters into the dielectric but with the metal replaced by a negative-index metamaterial (NIMM) [16]. Here excitations are not SPPs but surface polaritons (SPs), i.e., surface electromagnetic waves propagating along a dielectric-NIMM interface. By using electromagnetically induced transparency (EIT), it was shown that the SPs have a very small attenuation. References [17,18] extended this scheme for obtaining a large cross-phase modulation (CPM) and hence realizing large phase shifts or maximum entangled states of two optical pulses. However, to obtain low-loss SPs and large CPM predicted in Refs. [16–18], a very low room-temperature condition is needed.

In this article we propose a scheme to realize stable propagation of linear and nonlinear SPs. The system we suggest is a planar waveguide superposed by two-layer media (one is a NIMM and the other is a dielectric) working at room temperature, where N-type four-level quantum emitters are placed at the interface between the two media and interact with three (pump, signal, and control) laser fields through an active Raman gain (ARG) [19] mechanism. Our findings include two aspects. (i) In the linear propagation regime SPs can acquire an ARG from the pump field and a gain doublet appears in the gain spectrum of the signal field induced by the quantum interference effect from the control field. The ARG can be used not only to completely compensate the Ohmic loss in the NIMM but also to get a superluminal group velocity for the SPs [20]. (ii) In the nonlinear propagation regime a huge enhancement of Kerr nonlinearity of the SPs can be obtained. As a consequence, ARG-assisted $(1+1)$-dimensional [$(1+1)$D] and $(2+1)$D superluminal surface polaritonic solitons with extremely low generation power may be created based on the strong confinement of the electric field at the dielectric-NIMM interface. The results predicted here may have potential applications in light information processing and transmission at the nanoscale level.

Note that our work is different from Refs. [3–8,12–15], where only linear SPPs were considered. It is also different from Refs. [16–18], where the excitation scheme is based on EIT. Here we explore both the linear and nonlinear SPs excited along the NIMM-dielectric interface rather than the metal-dielectric one. At variance with the EIT scheme, where the signal field operates in an absorption mode and hence its attenuation still exists, in our ARG scheme the signal field operates in a stimulated Raman emission mode, which leads to different propagation characteristics without loss and the system can work at room temperature.

The rest of the article is arranged as follows. In Sec. II we describe our theoretical model. In Sec. III we discuss superluminal SPs via ARG at the linear level. In Sec. IV we investigate the nonlinear dynamics of the superluminal SPs and show that the system possesses a huge Kerr nonlinearity and

*gxhuang@phy.ecnu.edu.cn

supports $(1+1)$D superluminal surface polaritonic solitons. In Sec. V we show that $(2+1)$ superluminal polaritonic solitons can also be obtained. Finally, in Sec. VI we summarize the main results obtained in this work.

II. MODEL

Consider a planar waveguide superposed by a NIMM in the lower half plane $z<0$ (with permittivity ε_1 and permeability μ_1) and a dielectric in the upper half $z>0$ (with permittivity ε_2 and permeability μ_2) [Fig. 1(a)]. Quantum emitters denoted by black dots (they may be atoms, quantum dots, etc.) with an N-type level configuration are doped in the thin layer of the dielectric near the NIMM-dielectric interface and interact with three (pump, signal, and control) laser fields with angular frequency ω_p, ω_s, and ω_c, respectively (the inset of Fig. 1). The $|j\rangle$ $(j=1,2,3,4)$ are the energy levels of the quantum emitters and the Δ_j $(j=2,3,4)$ are the corresponding detunings. The energy levels $|1\rangle$, $|2\rangle$, and $|3\rangle$ combined with the pump and control fields constitute a typical ARG core [19]. Surface polaritons are excited at the NIMM-dielectric interface and propagate in the positive x direction.

Different from metal-dielectric interfaces where only the transverse magnetic (TM) mode is allowed [1], the present system supports both the TM mode and the transverse electric mode [16]. For simplicity we consider only the TM mode here. Solving Maxwell equations in the absence of the quantum emitters, one obtains the expression of the TM mode

$$\mathbf{E}(\mathbf{r},t)=\begin{cases}(k\mathbf{e}_z-ik_2\mathbf{e}_x)\frac{c}{\varepsilon_2\omega_l}\sqrt{\frac{\hbar\omega_l}{\varepsilon_0 L_x L_y L_z}}\hat{a}(\omega_l)e^{-k_2 z+i(kx-\omega_l t)}+\text{c.c.}, & z>0\\ (k\mathbf{e}_z+ik_1\mathbf{e}_x)\frac{c}{\varepsilon_1\omega_l}\sqrt{\frac{\hbar\omega_l}{\varepsilon_0 L_x L_y L_z}}\hat{a}(\omega_l)e^{k_1 z+i(kx-\omega_l t)}+\text{c.c.}, & z<0,\end{cases} \tag{1}$$

where $\mathbf{e}_x$ ($\mathbf{e}_z$) is the unit vector along the x (z) direction, ω_l is the oscillating frequency, $k_\alpha^2=k^2-\omega_l^2\varepsilon_\alpha\mu_\alpha/c^2$ satisfies the relation $k_1\varepsilon_2=-k_2\varepsilon_1$, L_x (L_y) is the length of the NIMM-dielectric interface along the x (y) direction, L_z is the mode length in the z direction with the expression given by Eq. (A3), $k=k(\omega_l)=(\omega_l/c)[\varepsilon_1\varepsilon_2(\varepsilon_1\mu_2-\varepsilon_2\mu_1)/(\varepsilon_1^2-\varepsilon_2^2)]^{1/2}$ is the propagation constant of the SP mode, and $\hat{a}(\omega_l)$ is the creation operator of TM photons (see Appendix A for details). We assume the photon numbers in all three laser fields are much larger than one, so $\hat{a}(\omega_l)$ can be taken as the c-number $a(\omega_l)$.

The Drude model is chosen to describe the permittivity and permeability of the NIMM, i.e., $\varepsilon_1=\varepsilon_1(\omega_l)\equiv\varepsilon_\infty-\omega_e^2/[\omega_l(\omega_l+i\gamma_e)]$ and $\mu_1=\mu_1(\omega_l)\equiv\mu_\infty-\omega_m^2/[\omega_l(\omega_l+i\gamma_m)]$. Here ω_e (γ_e) is the electric plasma frequency (decay rate), ω_m (γ_m) is the magnetic plasma frequency (decay rate), and ε_∞ and μ_∞ are background constants. At variance with conventional metal-dielectric interfaces, the SP loss along the NIMM-dielectric interface can be largely suppressed and even a lossless point [i.e., the point with $\text{Im}(k)=0$] exists for a particular value of ω_l due to the destructive interference between electric and magnetic responses [16], shown as the blue solid line for the NIMM and black dash-dotted line for the metal in Fig. 2. The system parameters are given by [16] $\varepsilon_2=1$, $\mu_2=1$, $\varepsilon_\infty=6.5$, $\mu_\infty=6.5$, $\omega_e=1.37\times10^{16}$ s^{-1}, $\gamma_e=2.37\times10^{13}$ s^{-1} (as for Ag), $\omega_m=10^{15}$ s^{-1}, and $\gamma_m=10^{12}$ s^{-1}.

Unfortunately, the suppression of the SP loss is always accompanied by a deconfinement of the SP in the dielectric [i.e., $\text{Re}(1/k_2)\to\infty$ when $\text{Im}(k)\to0$], shown as the red dashed and blue solid lines in Fig. 2. To obtain an acceptable suppression of the SP loss and a required SP confinement simultaneously, one is forced to select an appropriate excitation frequency ω_l that has a small deviation from the lossless point. As a result, a small SP loss still exists [16–18]. One aim of the present work is to show that this small SP loss can be eliminated completely in our system (see Sec. III below).

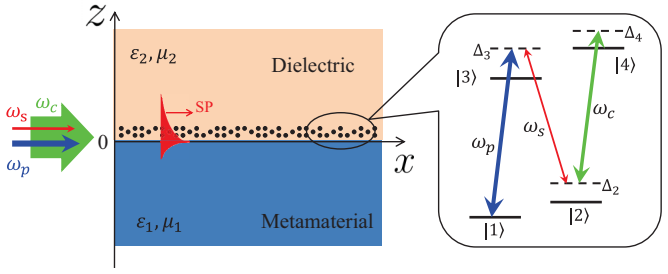

FIG. 1. (Color online) Surface polaritons excited via ARG at the interface between a NIMM (with permittivity ε_1 and permeability μ_1 in the region $z<0$) and the dielectric (with permittivity ε_2 and permeability μ_2 in the region $z>0$). the inset shows the energy-level diagram and ARG excitation scheme for the N-type quantum emitters (denoted by black dots) doped in the dielectric near the interface. Here ω_p (ω_c,ω_s) is the angular frequency of the pump, control, and signal field and Δ_j is the detuning, with $j=2,3,4$, respectively.

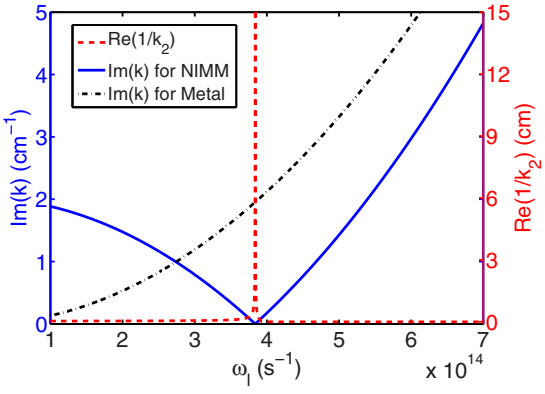

FIG. 2. (Color online) The $\text{Im}(k)$ of the SP in the NIMM (blue solid line) and metal (black dash-dotted line) and the $\text{Re}(1/k_2)$ of the electric field in the dielectric over the NIMM (red dashed line) as functions of optical oscillating frequency ω_l.

We now derive the equations of motion describing the resonant interaction between the TM mode and the four-level quantum emitters (hereafter we assume they are atomic gases for simplicity) with an N-type level configuration, in which the pump field couples the levels $|1\rangle$ and $|3\rangle$, the signal field couples the levels $|2\rangle$ and $|3\rangle$, and the control field couples the levels $|2\rangle$ and $|4\rangle$ (Fig. 1). For simplicity, we assume that the pump, signal, and control fields belong to the TM mode given by Eq. (1). Thus we have $\mathbf{E}(\mathbf{r},t)=\sum_{l=p,c,s}\mathcal{E}_l\mathbf{u}_l(z)e^{i[k(\omega_l)x-\omega_l t]}+\text{c.c.}$, with $\mathcal{E}_l=(\hbar\omega_l/\varepsilon_0 L_x L_y L_z)^{1/2}a(\omega_l)$ and $\mathbf{u}_l(z)=c[k(\omega_l)\mathbf{e}_z-ik_2(\omega_l)\mathbf{e}_x]e^{-k_2(\omega_l)z}/\varepsilon_2\omega_l$.

Under the rotating-wave approximation, the Hamiltonian of the system in the interaction picture reads

$$H_{\text{int}}=-\hbar\left[\sum_{j=1}^{4}\Delta_j|j\rangle\langle j|+\zeta_p(z)\Omega_p|3\rangle\langle 1|+\zeta_s(z)\Omega_s|3\rangle\langle 2|+\zeta_c(z)\Omega_c|4\rangle\langle 2|+\text{H.c.}\right], \tag{2}$$

where $\Delta_1=0$, $\Delta_2=\omega_p-\omega_s-(E_2-E_1)/\hbar$, $\Delta_3=\omega_p-(E_3-E_1)/\hbar$, and $\Delta_4=\omega_c+\omega_p-\omega_s-(E_4-E_1)/\hbar$ are detunings (with E_j the eigenenergy of the state $|j\rangle$); $\zeta_c(z)\approx\zeta_s(z)\approx\zeta_p(z)=\mathbf{e}_{23}\cdot\mathbf{u}_s(z)\equiv\zeta(z)$ (because $\omega_c\approx\omega_s\approx\omega_p$); $\mathbf{e}_{ij}$ is the unit vector of the electric dipole matrix element $\mathbf{p}_{ij}$ associated with the transition from state $|i\rangle$ to state $|j\rangle$, i.e., $\mathbf{p}_{ij}=\mathbf{e}_{ij}p_{ij}$; and $\Omega_p=|\mathbf{p}_{31}|\mathcal{E}_p/\hbar$, $\Omega_s=|\mathbf{p}_{32}|\mathcal{E}_s/\hbar$, and $\Omega_c=|\mathbf{p}_{42}|\mathcal{E}_c/\hbar$ are the half Rabi frequencies of the pump, signal, and control fields with the amplitudes $\mathcal{E}_p$, $\mathcal{E}_s$, and $\mathcal{E}_c$, respectively. The motion of atoms is governed by the Bloch equation

$$i\hbar\left(\frac{\partial}{\partial t}+\Gamma\right)\sigma=[H_{\text{int}},\sigma], \tag{3}$$

where σ is a 4×4 density matrix in the interaction picture and Γ is a 4×4 relaxation matrix describing the spontaneous emission and dephasing of the system. Explicit expressions of Eq. (3) are presented in Appendix B.

The evolution of the electric field in the system is controlled by the Maxwell equation $\nabla^2\mathbf{E}-(1/c^2)\partial^2\mathbf{E}/\partial t^2=(1/\varepsilon_0c^2)\partial^2\mathbf{P}/\partial t^2$ with the electric polarization intensity given by

$$\mathbf{P}(\mathbf{r},t)=\mathcal{N}_a\int_{-\infty}^{\infty}dv f(v)(\mathbf{p}_{13}\sigma_{31}e^{i(k_px-\omega_pt)}+\mathbf{p}_{23}\sigma_{32}e^{i(k_sx-\omega_st)}+\mathbf{p}_{24}\sigma_{42}e^{i(k_cx-\omega_ct)}+\text{c.c.}), \tag{4}$$

where $\mathcal{N}_a$ is atomic density and $f(v)=1/\sqrt{\pi}v_T\exp[-(v/v_T)^2]$ is the velocity distribution function, with $v_T=(2k_BT/M)^{1/2}$ the most probable atomic speed at temperature T. The Doppler width defined by $\Delta\omega_D\equiv k_sv_T$ is usually adopted to derive analytic expressions without losing the validity of the analysis. Under the slowly varying envelope approximation the Maxwell equation reduces to

$$i\left(\frac{\partial}{\partial x}+\frac{1}{n_{\text{eff}}c}\frac{\partial}{\partial t}\right)\Omega_s+\kappa_{23}\int_{-\infty}^{\infty}dv f(v)\langle\sigma_{32}\rangle=0, \tag{5}$$

where $\kappa_{23}=\mathcal{N}_a\omega_s|\mathbf{p}_{32}|^2/2\hbar\varepsilon_0c$, c is the light speed in vacuum, and $n_{\text{eff}}=ck_s(\omega_s)/\omega_s$ is the effective refraction index. The average in the second term is defined by $\langle\psi(z)\rangle\equiv\int_{-\infty}^{+\infty}dz\,\zeta^*(z)\psi(z)/\int_{-\infty}^{+\infty}dz|\zeta(z)|^2$.

III. SURFACE POLARITONS VIA ARG THE IN LINEAR PROPAGATION REGIME

We first study the linear excitations, i.e., SPs, of the system. To this end, we must know the base state of the Maxwell-Bloch (MB) equations (3) and (5). The base state is the state in the absence of the signal field $\Omega_s=0$ and $\partial/\partial t=0$. Then the base state reads

$$\sigma_{11}^{(0)}=\frac{\Gamma_{14}|\zeta(z)\Omega_c|^2[\Gamma_3X_{31}+|\zeta(z)\Omega_p|^2]}{D}, \tag{6a}$$

$$\sigma_{22}^{(0)}=\frac{\Gamma_{23}|\zeta(z)\Omega_p|^2[\Gamma_4X_{42}+|\zeta(z)\Omega_c|^2]}{D}, \tag{6b}$$

$$\sigma_{33}^{(0)}=\frac{\Gamma_{14}|\zeta(z)\Omega_c|^2|\zeta(z)\Omega_p|^2}{D}, \tag{6c}$$

$$\sigma_{44}^{(0)}=\frac{\Gamma_{23}|\zeta(z)\Omega_c|^2|\zeta(z)\Omega_p|^2}{D}, \tag{6d}$$

$$\sigma_{31}^{(0)}=-\frac{\zeta(z)\Omega_p}{d_{31}}\frac{\Gamma_{14}\Gamma_3X_{31}|\zeta(z)\Omega_c|^2}{D}, \tag{6e}$$

$$\sigma_{42}^{(0)}=-\frac{\zeta(z)\Omega_c}{d_{42}}\frac{\Gamma_{23}\Gamma_4X_{42}|\zeta(z)\Omega_p|^2}{D}, \tag{6f}$$

with $X_{31}\equiv|d_{31}|^2/2\gamma_{31}$, $X_{42}\equiv|d_{42}|^2/2\gamma_{42}$, and $D\equiv\Gamma_{14}|\zeta(z)\Omega_c|^2[\Gamma_3X_{31}+2|\zeta(z)\Omega_p|^2]+\Gamma_{23}|\zeta(z)\Omega_p|^2[\Gamma_4X_{42}+2|\zeta(z)\Omega_c|^2]$.

We now focus on the linear excitation of the system: When the signal field is switched on, the system will involve into a time-dependent state. In the linear regime, i.e., at the first order of Ω_s, the population and the coherence between both the states $|1\rangle$ and $|3\rangle$ and the states $|2\rangle$ and $|4\rangle$ are not changed. The linear excitation of the system can be obtained by linearizing the MB equations (3) and (5) around the base state. By taking $\sigma_{jl}=\sigma_{jl}^{(0)}+\epsilon\sigma_{jl}^{(1)}$ and $\Omega_s=\epsilon\Omega_s^{(1)}$, where ϵ is a small parameter denoting the typical amplitude of Ω_s, we obtain the linear (first-order) solution $\Omega_s^{(1)}=Fe^{i\phi}$, $\sigma_{32}^{(1)}=a_{32}^{(1)}\zeta(z)Fe^{i\phi}$, $\sigma_{21}^{*(1)}=a_{21}^{*(1)}\zeta(z)Fe^{i\phi}$, $\sigma_{43}^{*(1)}=a_{43}^{*(1)}\zeta(z)Fe^{i\phi}$, and $\sigma_{41}^{*(1)}=a_{41}^{*(1)}\zeta(z)Fe^{i\phi}$, with other $\sigma_{jl}^{(1)}=0$. Here F is a constant, $\phi=K(\omega)x-\omega t$ [21], and

$$K=\frac{\omega}{n_{\text{eff}}c}+\kappa_{23}\int_{-\infty}^{\infty}dv f(v)\left\langle\zeta(z)\frac{B(\sigma_{33}^{(0)}-\sigma_{22}^{(0)})-[D_p+|\zeta(z)\Omega_c|^2]\zeta(z)\Omega_p\sigma_{31}^{*(0)}-[D_c+|\zeta(z)\Omega_p|^2]\zeta(z)\Omega_c\sigma_{42}^{*(0)}}{(\omega+d_{32})B-|\zeta(z)\Omega_p|^2[D_p+|\zeta(z)\Omega_c|^2]-|\zeta(z)\Omega_c|^2[D_c+|\zeta(z)\Omega_p|^2]}\right\rangle \tag{7}$$

is the linear dispersion relation of the excitation, with $D_c\equiv(\omega-d_{21}^*)(\omega-d_{41}^*)-|\zeta(z)\Omega_c|^2$, $D_p\equiv(\omega-d_{41}^*)(\omega-d_{43}^*)-|\zeta(z)\Omega_p|^2$, and $B\equiv(\omega-d_{21}^*)(\omega-d_{41}^*)(\omega-d_{43}^*)-(\omega-d_{21}^*)|\zeta(z)\Omega_p|^2-(\omega-d_{43}^*)|\zeta(z)\Omega_c|^2$. The explicit expressions of $a_{32}^{(1)}$, $a_{21}^{*(1)}$, $a_{43}^{*(1)}$, and $a_{41}^{*(1)}$ are given in Appendix C.

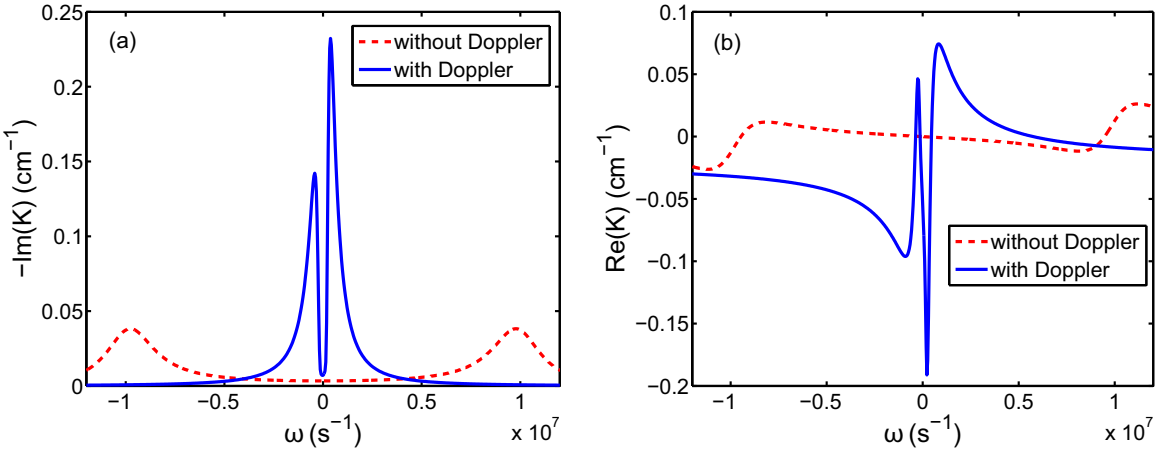

FIG. 3. (Color online) Linear dispersion relation of SPs: (a) $-\mathrm{Im}(K)$ and (b) $\mathrm{RK}(K)$ as functions of ω. The blue solid (red dashed) line is for the case with (without) the Doppler effect.

In Figs. 3(a) and 3(b), $-\mathrm{Im}(K)$ (characterizing the gain spectrum) and $\mathrm{Re}(K)$ (characterizing the refractive index) are plotted as functions of ω. In both panels, the blue solid (red dashed) line is for the case with (without) the Doppler effect. The system parameters are given by $\Gamma_3 = \Gamma_4 = 6\,\mathrm{MHz}$, $\Gamma_{13} = \Gamma_{23} = \Gamma_{14} = \Gamma_{24} = \Gamma_3/2$, $\gamma_{21} = 1\,\mathrm{kHz}$, $\Delta_2 = \Delta_4 = 0$, $\Delta_3 = 2\,\mathrm{GHz}$, $\Omega_p = 3\,\mathrm{MHz}$, $\Omega_c = 10\,\mathrm{MHz}$, $\Delta\omega_D = 250\,\mathrm{MHz}$, and $\kappa_{23} = 5 \times 10^{10}\,\mathrm{s^{-1}\,cm^{-1}}$.

We see from Fig. 3(a) that when the Doppler effect is absent the gain spectrum displays a gain doublet in which the width between the two peaks of the doublet is very wide (the red dashed line). However, when the Doppler effect is present the width of the doublet becomes very narrow and the peaks become asymmetric and are amplified significantly (the blue dashed line). Such a gain property can be used to compensate the Ohmic loss near the lossless point of $\mathrm{Im}(k)$ described in the preceding section.

From Fig. 3(b) we see that the system has an abnormal dispersion near $\omega = 0$ [i.e., $\partial\,\mathrm{Re}(K)/\partial\omega < 0$] and the dispersion property is quite different for the cases with and without the Doppler effect. In the presence of the Doppler effect, $\mathrm{Re}(K)$ has a much steeper slope near $\omega = 0$ than that without the Doppler effect, which means that the superluminal effect can be largely enhanced by the Doppler effect.

The physical reason for the property of the linear dispersion relation of the system described above is the following. Due to the Doppler effect, atoms with different velocities have different contributions to the gain spectrum. After the Doppler averaging, all contributions result in constructive interference. As a result, the two peaks in the gain spectrum are narrowed and greatly amplified. Furthermore, due to the large detuning Δ_3, the weights for the thermal motion of different atoms change very much, which results in the breaking of the gain spectrum's symmetry.

IV. SURFACE POLARITONS VIA ARG IN THE NONLINEAR PROPAGATION REGIME

A. Nonlinear envelope equation and giant Kerr nonlinearity

We now investigate the nonlinear excitations, in particular superluminal optical solitons, of the system. For this aim, we take the asymptotic expansion [22] $\sigma_{jl} - \sigma_{jl}^{(0)} = \sum_m \epsilon^m \sigma_{jl}^{(m)}$ and $\Omega_s = \sum_m \epsilon^m \Omega_s^{(m)}$, where all quantities on the right-hand side of the asymptotic expansion are considered as functions of the multiscale variables $x_m = \epsilon^m x$ ($m = 0,1,2$) and $t_m = \epsilon^m t$ ($m = 0,1$). Substituting the expansion into the MB equations, we obtain a series of linear but inhomogeneous equations for $\sigma_{ij}^{(m)}$ and $\Omega_s^{(m)}$ ($m = 1,2,3,4$), which can be solved order by order.

The zeroth-order ($m = 0$) and the first-order ($m = 1$) solutions are the same as that given in the preceding section, by now $\phi = K(\omega)x_0 - \omega t_0$ and F is the yet to be determined envelope function of the slow variables t_1, x_1, and x_2. In the second order ($m = 2$), a divergence-free solution for $\Omega_s^{(2)}$ gives the solvability condition

$$i\left(\frac{\partial}{\partial x_1}F + \frac{1}{V_g}\frac{\partial}{\partial t_1}F\right) = 0, \tag{8}$$

which means that F travels with group velocity $V_g \equiv (\partial K/\partial\omega)^{-1}$. Explicit expressions of the second-order solution are given in Appendix D.

In the third order ($m = 3$) the solvability condition for $\Omega_s^{(3)}$ requires

$$i\frac{\partial F}{\partial x_2} - \frac{1}{2}K_2\frac{\partial^2 F}{\partial t_1^2} - W|F|^2 F e^{-2\bar{\alpha}x_2} = 0, \tag{9}$$

where $\bar{\alpha} = \varepsilon^2\mathrm{Im}(K)$, $K_2 = \partial^2 K/\partial\omega^2$ is the coefficient characterizing group-velocity dispersion, and

$$W = \kappa_{23}\int_{-\infty}^{\infty} dv f(v)\left\langle \zeta(z)|\zeta(z)|^2 \frac{B\left(a_{22}^{(2)} - a_{33}^{(2)}\right) + [D_p + |\zeta(z)\Omega_c|^2]\zeta(z)\Omega_p a_{31}^{*(2)} + [D_c + |\zeta(z)\Omega_p|^2]\zeta(z)\Omega_c a_{42}^{*(2)}}{(\omega + d_{32})B - |\zeta(z)\Omega_p|^2[D_p + |\zeta(z)\Omega_c|^2] - |\zeta(z)\Omega_c|^2[D_c + |\zeta(z)\Omega_p|^2]}\right\rangle \tag{10}$$

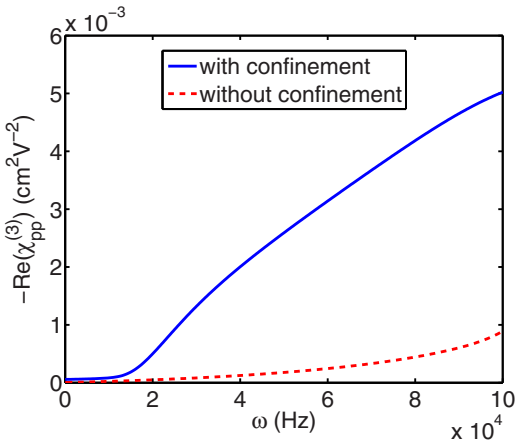

FIG. 4. (Color online) Giant Kerr nonlinearity. Third-order optical susceptibility $-\mathrm{Re}(\chi_{ss}^{(3)})$ as a function of ω with confinement (blue solid line) and with no confinement (red dashed line).

is the coefficient characterizing the self-phase modulation of the signal field. The third-order nonlinear optical susceptibility $\chi_{ss}^{(3)}$ is proportional to W via the relation

$$\chi_{ss}^{(3)} = \frac{2c}{\omega_s}\frac{|\mathbf{p}_{23}|^2}{\hbar^2}W. \tag{11}$$

Shown in Fig. 4 is $-\mathrm{Re}(\chi_{ss}^{(3)})$ as a function of ω when there is confinement [i.e., with the mode modulation $\zeta(z)$, the blue solid line] and no confinement [i.e., $\zeta(z) = 1$, the red dashed line]. The system parameters are chosen to be the same as those used in Fig. 3, but here $\Omega_c = 20$ MHz. We see that $|\mathrm{Re}(\chi_{ss}^{(3)})|$ is significantly enhanced due to the light confinement near the NIMM-dielectric interface. Typically, we have

$$\mathrm{Re}(\chi_{ss}^{(3)}) = -5.02 \times 10^{-3}\ \mathrm{cm}^2\,\mathrm{V}^{-2} \tag{12}$$

for $\omega = 1.0 \times 10^5\ \mathrm{s}^{-1}$. This value corresponds to the Kerr coefficient $n_2 = 3\,\mathrm{Re}(\chi_{ss}^{(3)})/[2(1+2cK/\omega_s)^{1/2}] = -7.53 \times 10^{-3}\ \mathrm{cm}^2\,\mathrm{V}^{-2}$. Hence the system possesses a giant Kerr nonlinearity, which is very useful for practical applications of nonlinear optics, e.g., the formation of surface polaritonic solitons, as described below. Combining the solvability conditions at the second and third orders, we obtain the dimensional envelope equation

$$i\frac{\partial}{\partial x}U - \frac{1}{2}K_2\frac{\partial^2 U}{\partial \tau^2} - W|U|^2 U e^{-2\alpha x} = 0, \tag{13}$$

with $\tau = t - x/V_g$ and $U = \epsilon F$.

B. Superluminal surface polaritonic solitons

Since Eq. (13) obtained above has complex coefficients, i.e., it is a Ginzberg-Landau equation, it does not allow a stable soliton solution in general. However, as shown below, we can find a realistic parameter set under the ARG condition to make the imaginary parts of these coefficients much smaller than their corresponding real parts. Thus shape-preserving nonlinear localized solutions that can propagate a long distance without a significant distortion are available.

For an analytical analysis, we first neglect the small imaginary parts of the coefficients and take $\omega = 0$. Then Eq. (13) can be converted into the dimensionless form

$$i\frac{\partial}{\partial s}u + \frac{\partial^2}{\partial \sigma^2}u + 2|u|^2 u = 0, \tag{14}$$

with $s = -x/2L_D$, $\sigma = \tau/\tau_0$, and $u = U/U_0$. Here τ_0 is a typical pulse duration, $L_D = \tau_0^2/\widetilde{K}_2$ is a typical dispersion length, and $U_0 = (\widetilde{K}_2/\widetilde{W})^{1/2}/\tau_0$ is a typical half Rabi frequency of the signal field, with $\widetilde{K}_2$ and $\widetilde{W}$ the real parts of $K_2 = (\partial^2 K/\partial\omega^2)|_{\omega=0}$ and $W|_{\omega=0}$, respectively. A single-soliton solution in terms of the half Rabi frequency is

$$\Omega_s = [(\widetilde{K}_2/\widetilde{W})^{1/2}/\tau_0]\mathrm{sech}[(t - x/\widetilde{V}_g)/\tau_0] \times \exp[i(\widetilde{K}_0 + 1/2L_D)x],$$

with $\widetilde{K}_0 = \mathrm{Re}(K)|_{\omega=0}$, which describes a bright soliton traveling with the propagating velocity $\widetilde{V}_g = [\mathrm{Re}(\partial K/\partial\omega)]^{-1}|_{\omega=0}$. The corresponding signal field is a surface polaritonic soliton with the form

$$\mathbf{E}_s(\mathbf{r},t) = \frac{\hbar}{|\mathbf{p}_{23}|\tau_0}\sqrt{\frac{\widetilde{K}_2}{\widetilde{W}}}\,\mathbf{u}_s(z)\mathrm{sech}\left[\frac{1}{\tau_0}\left(t - \frac{x}{\widetilde{V}_g}\right)\right] \times \exp\left\{i\left[\left(k(\omega_s) + K(\omega) + \frac{1}{2L_D}\right)x - (\omega_s + \omega)t\right]\right\} + \mathrm{c.c.} \tag{15}$$

We see that the total absorption of the surface polaritonic soliton is given by $\mathrm{Im}[k(\omega_s) + K(\omega)]$. As indicated in Sec. II, to obtain light-field confinement one should choose ω_s to deviate from the lossless point (i.e., the point $\mathrm{Im}[k(\omega_s)] = 0$) so $\mathrm{Im}[k(\omega_s)] > 0$, i.e., the Ohmic loss of the system is unavoidable if the quantum emitters are not used. In our system, the Ohmic loss can be completely eliminated by using the quantum emitters under the ARG condition because $\mathrm{Im}K(\omega) < 0$ for a nonzero ω. That is to say,

$$\mathrm{Im}[k(\omega_s) + K(\omega)] \approx 0. \tag{16}$$

Consequently, the problem between the confinement and the suppression of the Ohmic loss, which is usually needed to be traded off, is solved in our system. As a result, the linear and nonlinear surface polaritons can propagate for a fairly long distance (about 1 cm) with nearly no absorption.

We now give a realistic parameter set for the formation of a lossless surface polaritonic soliton. For a ^{85}Rb atomic vapor, we choose $\Omega_p = 3$ MHz, $\Omega_c = 8$ MHz, $\Delta_3 = 2.0 \times 10^9\ \mathrm{s}^{-1}$, $\tau_0 = 1.0 \times 10^{-6}$ s, $\omega_s = 3.84 \times 10^{14}\ \mathrm{s}^{-1}$, $\Delta_4 = 0\ \mathrm{s}^{-1}$, and $\Delta_2 = 4.01 \times 10^4\ \mathrm{s}^{-1}$ and the other parameters are the same as those given above. Then we obtain $\mathrm{Im}(k) = 0.183\ \mathrm{cm}^{-1}$ and $\mathrm{Im}(K) = -0.182\ \mathrm{cm}^{-1}$ and hence $\mathrm{Im}(k+K) = 0.001\ \mathrm{cm}^{-1}$. Furthermore, we have $K_2 = -(8.23 + 0.20i) \times 10^{-11}\ \mathrm{cm}^{-1}\,\mathrm{s}^2$, $W = -(9.11 + 0.036i) \times 10^{-15}\mathrm{cm}^{-1}\,\mathrm{s}^2$, $L_D = L_{NL} = 0.92$ cm, and $U_0 = 9.5 \times 10^7\ \mathrm{s}^{-1}$. One can see that the imaginary parts of K_2 and W are indeed much smaller than their corresponding real parts. The physical reason for such small imaginary parts is contributed by the quantum interference effect contributed by the control field.

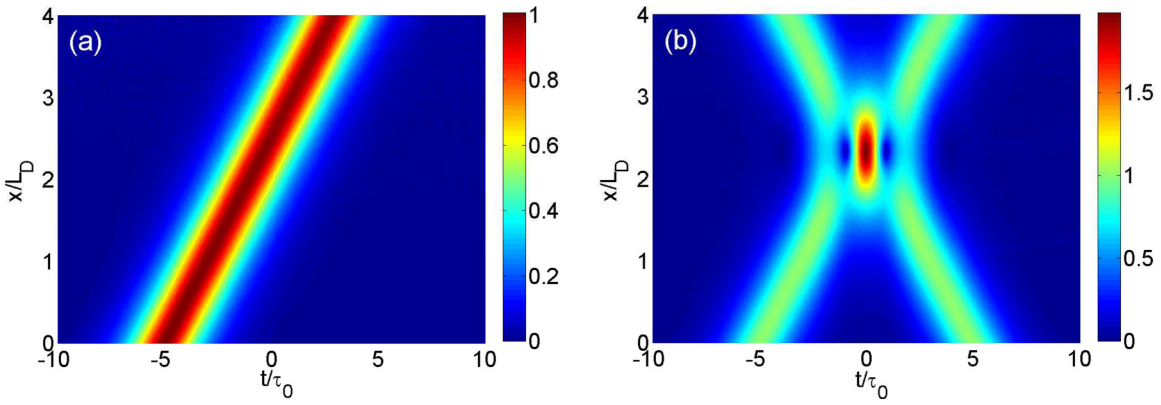

FIG. 5. (Color online) Propagation and interaction of superluminal surface polaritonic solitons: (a) wave shape $|\Omega_s/U_0|^2$ for a superluminal surface polaritonic soliton as a function of x/L_D and t/τ_0 and (b) collision between two superluminal surface polaritonic solitons.

Using the above, we obtain the propagating velocity of the surface polaritonic soliton

$$\widetilde{V}_g \approx -2.17 \times 10^{-4} c, \tag{17}$$

which means that the surface polaritonic soliton travels with a superluminal velocity. The threshold of the optical power density $\bar{P}_{\max}$ for generating the superluminal surface polaritonic soliton can be calculated by using Poynting's vector [22]. We obtain

$$\bar{P}_{\max} = 2.61\ \mu\text{W}. \tag{18}$$

Thus, very low input power is needed to generate the surface polaritonic soliton. The reason for such low generation power is the giant Kerr nonlinearity of the system, also contributed by the quantum interference effect contributed by the control field.

The stability of the superluminal surface polaritonic soliton is checked by using a numerical simulation. Figure 5(a) shows the wave shape of $|\Omega_s/U_0|^2$ as a function of x/L_D and t/τ_0. The result is obtained by numerically solving Eq. (13) with full complex coefficients taken into account. We see that the soliton remains almost unchanged for propagation distances up to 4 cm, and much longer than that (several millimeters) for the linear surface polariton obtained in Ref. [16].

A simulation of the collision between two superluminal surface polaritonic solitons is also carried out, with the result presented in Fig. 5(b). We see that the two solitons keep their identity after the collision.

V. THE (2 + 1)D SUPERLUMINAL SURFACE POLARITONIC SOLITONS

In the discussion given above, an assumption was implicated in Eq. (5), i.e., the motion of the SPs is independent of the transverse coordinate y, which is valid only for the probe pulse with large transverse spatial width. Because the NIMM-dielectric interface is a plane, such an assumption will be broken if the transverse width of the pulse is small. In this case Eq. (5) is replaced by

$$i\left(\frac{\partial}{\partial x}+\frac{1}{n_{\text{eff}}c}\frac{\partial}{\partial t}\right)\Omega_s+\frac{c}{2\omega_s}\left(\frac{\partial^2}{\partial x^2}+\frac{\partial^2}{\partial y^2}\right)\Omega_s + \kappa_{23}\int_{-\infty}^{\infty} dv f(v)\langle\sigma_{32}\rangle = 0, \tag{19}$$

i.e., the diffraction effect must be taken into account.

To obtain stable polaritonic solitons in 2 + 1 dimensions, we assume that the half Rabi frequency of the control field is spatially modulated with $\Omega_c = \Omega_c^{(0)}[1+\epsilon^2\Omega_c^{(2)}(y)]$, where $\Omega_c^{(0)}$ is a constant and $\Omega_c^{(2)}(y)$ is a slowly varying function of y [i.e., $\Omega_c^{(2)}(y_1)$ with $y_1 = \epsilon y$]. Then the envelope equation (13) is replaced by

$$i\frac{\partial}{\partial x}U-\frac{1}{2}K_2\frac{\partial^2 U}{\partial\tau^2}+\frac{c}{2\omega_s}\frac{\partial^2 U}{\partial y^2}-W|U|^2Ue^{-2\alpha x} + V(y)U = 0, \tag{20}$$

where

$$V(y) = \kappa_{23}\int_{-\infty}^{\infty} dv f(v)\left\langle\zeta(z)\frac{\zeta(z)\Omega_c^{(0)}\Omega_c^{(2)}(y)a_{43}^{*(1)} - [D_c+|\zeta(z)\Omega_p|^2]\zeta(z)\Omega_c^{(0)}\mathcal{P}_1 - \left[D_p+\left|\zeta(z)\Omega_c^{(0)}\right|^2\right]\zeta(z)\Omega_p\mathcal{P}_2}{(\omega+d_{32})B - |\zeta(z)\Omega_p|^2\left[D_p+\left|\zeta(z)\Omega_c^{(0)}\right|^2\right] - \left|\zeta(z)\Omega_c^{(0)}\right|^2[D_c+|\zeta(z)\Omega_p|^2]}\right\rangle, \tag{21}$$

with

$$\mathcal{P}_1 = \zeta^*(z)\Omega_c^{*(0)}\Omega_c^{*(2)}(y)\left[a_{32}^{(1)} - \zeta(z)\Omega_p a_{21}^{*(1)}/(\omega - d_{41}^*)\right]$$

and

$$\mathcal{P}_2 = \zeta(z)\Omega_c^{(0)}\Omega_c^{(2)}(y)a_{41}^{*(1)} + \left|\zeta(z)\Omega_c^{(0)}\right|^2\Omega_c^{*(2)}(y)a_{21}^{*(1)}/(\omega - d_{41}^*).$$

Expression (21) is an external potential contributed by the modulation part of the control field, which can be used to arrest the collapse of (2 + 1)D surface polaritonic solitons. Generally, the nonlinear coefficient W is y dependent [i.e., $W = W(y)$], with the expression of $W(y)$ the same as that given in (10). Because the populations in states $|2\rangle$ and $|4\rangle$ are very small, the contribution from $\Omega_c^{(2)}(y)$ is negligible, i.e., W has only a very weak dependence on y.

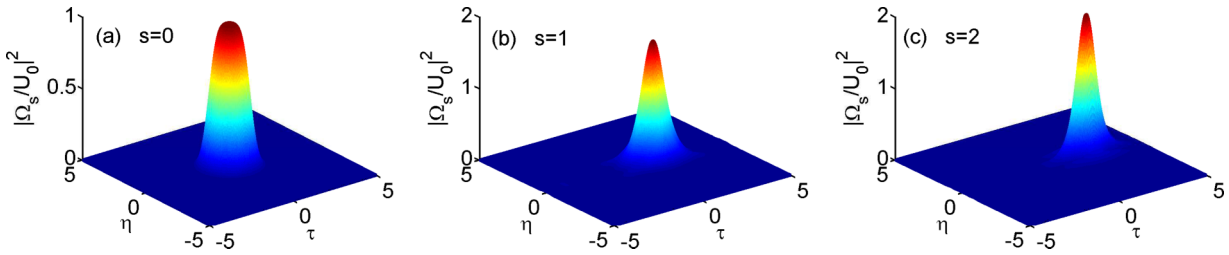

FIG. 6. (Color online) Propagation of (2 + 1)D superluminal surface polaritonic solitons by taking $|\Omega_s/U_0|^2$ as a function of η, τ, and s: (a) initial hyperbolic secant pulse at $s = 0$, (b) the (2 + 1)D surface polaritonic soliton by evolving the initial hyperbolic secant pulse to the distance $s = 1$, and (c) the (2 + 1)D surface polaritonic soliton at $s = 2$.

Neglecting the small imaginary part of the coefficients and taking $\omega = 0$, Eq. (20) can be written into the dimensionless form

$$i\frac{\partial u}{\partial s} + \frac{\partial^2 u}{\partial \sigma^2} + 2|u|^2 u - d_1\frac{\partial^2 u}{\partial \eta^2} - V'(\eta)u = 0, \qquad (22)$$

with $s = -x/2L_D$, $\sigma = \tau/\tau_0$, $\eta = y/R_y$, $u = U/U_0$, $d_1 = L_D/L_{\rm diff}$, and $V'(\eta) = 2L_D V(y)$. Here R_y is the spatial width of the probe pulse in the y direction and $L_{\rm diff} = \omega_s R_y^2/c$ is the characteristic diffraction length.

We give a realistic parameter set for the formation of a (2 + 1)D surface polaritonic soliton in the system. For a ^{85}Rb atomic vapor, we choose $\Omega_c^{(0)} = 9$ MHz, $\Omega_c^{(2)}(y) = 8\exp[-y^2/(2R_y)^2]$, $\tau_0 = 5.0 \times 10^{-7}$ s, $\Delta_2 = 4.09 \times 10^5$ s^{-1}, and $R_y = 100$ μm and the other parameters are the same as those given in the previous section. We obtain $K_2 = (2.93 - 0.83i) \times 10^{-13}$ cm^{-1} s^2, $W = (4.07 - 1.15i) \times 10^{-18}$cm^{-1} s^2, $V(y) = (-5.65 + 0.48i)\exp[-y^2/(2R_y)^2]$ cm^{-1}, $L_D = L_{NL} = 0.85$ cm, $L_{\rm diff} = 1.28$ cm, and $U_0 = 5.37 \times 10^8$ s^{-1}. One can see that the imaginary parts of K_2, W, and $V(y)$ are indeed much smaller than their corresponding real parts.

We numerically solve Eq. (22) by using a split-step Fourier method. Figure 6 shows the result of the signal-field intensity $|\Omega_s/U_0|^2$ as a function of η, τ_0, and s. In the numerical simulation a hyperbolic-secant-type initial pulse [i.e., $u = \mathrm{sech}(\tau^2 + \eta^2)$] is taken, as shown in Fig. 6(a). Plotted in Fig. 6(b) is the result of the signal field by evolving the initial pulse to the propagation distance $s = 1$. We see that the initial pulse is compressed in the η direction and the strength of the signal field increases, meaning that the initial pulse evolves to a (2 + 1)D surface polaritonic soliton. Illustrated in Fig. 6(c) is the signal field at the propagation distance $s = 2$. We see that the (2 + 1)D surface polaritonic soliton can indeed propagate stably for a fairly long distance.

VI. CONCLUSION

In recent years, nonlinear plasmon excitations propagating along dielectric-metal interfaces, i.e. surface plasmon solitons, have attracted much attention [23–27]. However, our work is different from Refs. [23–27] because what we considered here is a dielectric-NIMM interface doped with quantum emitters. Furthermore, the group-velocity dispersion effect of the SPs were taken into account in our work. In addition, the nonlinearity of our system comes from the resonance between the quantum emitters and the signal, pump, and control fields. Because the pump, signal, and control fields are weak and far from material resonances, both the dielectric and the NINM can be safely taken as linear optical materials.

Recently, a type of superluminal SP was discussed via a coherent population oscillation (CPO) [28]. The present ARG scheme suggested in the present work is very different from the CPO scheme of Ref. [28] and possesses many attractive advantages. The reasons are the following. (i) To acquire a gain in the CPO scheme some particular requirements are needed that are not easy to fulfill. In the present ARG scheme the system always has a gain. Due to the quantum interference effect (which is absent in the CPO scheme) contributed by the control field, the gain can be enlarged and can be used to completely eliminate the Ohmic loss in the NIMM. (ii) In the CPO scheme a harmful influence of the four-wave-mixing effect is hard to avoid, while in the ARG scheme such a mixing effect is absent. (iii) The Kerr nonlinearity obtained in the CPO scheme is much smaller than that in the ARG scheme. (iv) The superluminal polaritonic solitons in the ARG scheme are easier to realize and manipulate experimentally than in the CPO scheme.

Note that the experimental research of SPs excited in an air-NIMM interface has been carried out in the microwave regime [29] and recent efforts have moved to the optical frequency regime [30]. One outstanding work is the realization of a NIMM at 780 nm [31]. To experimentally realize the theoretical model and test the calculated results presented in our work, one can design an experimental setup with the geometry shown in Fig. 1. The SPs can be excited at the dielectric-NIMM interface via the technique of optical grating coupling or end-fire coupling [1]. In the dielectric region near the interface, dilute quantum emitters are doped. The pump, control, and signal fields are selected from the TM mode of the electric field that propagates along the x direction. Because the electric field decays exponentially away from both sides of the interface, stacking several layers or even one layer of the NIMM is enough.

In conclusion, we have suggested a scheme to realize stable propagation of linear and nonlinear SPs by placing N-type four-level quantum emitters at the interface between a dielectric and a NIMM. We have shown that in the linear propagation regime the SPs can acquire an ARG from a pump field and a gain doublet appears in the gain spectrum of the signal field induced by the quantum interference effect from a control field. The ARG can be used not only to completely compensate the Ohmic loss in the NIMM but also to acquire a superluminal group velocity for the SPs. We have also shown

that in the nonlinear propagation regime a huge enhancement of the Kerr nonlinearity of the SPs can be obtained. As a result, ARG-assisted (1 + 1)D and (2 + 1)D superluminal surface polaritonic solitons with extremely low generation power can be generated based on the strong confinement of the electric field at the dielectric-NIMM interface. The huge Kerr nonlinearity obtained here can also be used to realize some additional nonlinear optical processes and may have promising applications in light information processing and transmission at the nanoscale level based on the NIMM. Thus the present work opens an avenue for the research of nanotechnology nonlinear and quantum optics.

ACKNOWLEDGMENTS

This work was supported by the NSF China under Grants No. 11475063, No. 11174080, No. 11474099, and No. 11475063.

APPENDIX A: THE TM MODE OF THE ELECTROMAGNETIC FIELD

We assume that the SP propagates in the positive x direction. The form of TM mode of the electromagnetic (EM) field is $\mathbf{H}(\mathbf{r},t) = -\mathbf{e}_y H(z)e^{i\theta} + \text{c.c.}$ and $\mathbf{E}(\mathbf{r},t) = \mathbf{E}(z)e^{i\theta} + \text{c.c.}$, with $\theta = kx - \omega_l t$. Substitution of these expressions into Maxwell equations yields $\mathbf{E}(\mathbf{r},t) = (i/\varepsilon_0\varepsilon\omega_l)\{[dH(z)/dz]\mathbf{e}_x - ikH(z)\mathbf{e}_z\}e^{i\theta} + \text{c.c.}$ Here $H(z)$ satisfies the equation $\partial^2 H(z)/\partial z^2 + (\omega_l^2\varepsilon\mu/c^2 - k^2)H(z) = 0$, which can be solved in combination with the boundary conditions of the EM field. Then one obtains [16]

$$\mathbf{E}(\mathbf{r},t) = \begin{cases} (k\mathbf{e}_z + ik_1\mathbf{e}_x)\frac{A}{\varepsilon_0\varepsilon_1\omega_l}e^{k_1 z+i\theta} + \text{c.c.}, & z < 0 \\ (k\mathbf{e}_z - ik_2\mathbf{e}_x)\frac{A}{\varepsilon_0\varepsilon_2\omega_l}e^{-k_2 z+i\theta} + \text{c.c.}, & z > 0, \end{cases} \tag{A1a}$$

$$\mathbf{H}(\mathbf{r},t) = \begin{cases} -\mathbf{e}_y A e^{k_1 z+i\theta} + \text{c.c.}, & z < 0 \\ -\mathbf{e}_y A e^{-k_2 z+i\theta} + \text{c.c.}, & z > 0, \end{cases} \tag{A1b}$$

where A is an arbitrary constant, $\mathbf{e}_\alpha$ ($\alpha = x,y,z$) is the unit vector along the α direction, and $k_j^2 \equiv k^2 - \omega_l^2\varepsilon_j\mu_j/c^2$ ($j = 1$ for the NIMM and $j = 2$ for the dielectric) satisfies the relation $k_1\varepsilon_2 = -k_2\varepsilon_1$. The propagation constant of the SP is given by $k(\omega_l) = \omega_l[\varepsilon_1\varepsilon_2(\varepsilon_1\mu_2 - \varepsilon_2\mu_1)/(\varepsilon_1^2 - \varepsilon_2^2)]^{1/2}/c$.

The energy of the pulsed EM field can be expressed as $U = \frac{1}{2}\int\int\int dx\,dy\,dz(\varepsilon_0\tilde{\varepsilon}|\mathbf{E}|^2 + \mu_0\tilde{\mu}|\mathbf{H}|^2)$, with $\tilde{\varepsilon} \equiv \text{Re}[\partial(\omega_l\varepsilon)/\partial\omega_l]$ and $\tilde{\mu} \equiv \text{Re}[\partial(\omega_l\mu)/\partial\omega_l]$. Based on the above formula, we obtain a quantized electric field with the form

$$\mathbf{E}(\mathbf{r},t) = \begin{cases} (k\mathbf{e}_z + ik_1\mathbf{e}_x)\frac{c}{\varepsilon_1\omega_l}\sqrt{\frac{\hbar\omega_l}{\varepsilon_0 L_x L_y L_z}}\hat{a}(\omega_l)e^{k_1 z+i\theta} + \text{c.c.}, & z < 0 \\ (k\mathbf{e}_z - ik_2\mathbf{e}_x)\frac{c}{\varepsilon_2\omega_l}\sqrt{\frac{\hbar\omega_l}{\varepsilon_0 L_x L_y L_z}}\hat{a}(\omega_l)e^{-k_2 z+i\theta} + \text{c.c.}, & z > 0, \end{cases} \tag{A2}$$

where $\hat{a}(\omega_l)$ is the creation operator of TM photons, L_x and L_y are the lengths of the NIMM-dielectric interface in the x and y directions, respectively, and L_z is defined as

$$L_z \equiv \frac{1}{2}\left[\frac{\tilde{\varepsilon_1}}{|k_1|}\frac{c^2}{\omega_l^2}\frac{|k|^2 + |k_1|^2}{|\varepsilon_1|^2} + \frac{\tilde{\varepsilon_2}}{|k_2|}\frac{c^2}{\omega_l^2}\frac{|k|^2 + |k_2|^2}{|\varepsilon_2|^2}\right] + \frac{1}{2}\left(\frac{\tilde{\mu_1}}{|k_1|} + \frac{\tilde{\mu_2}}{|k_2|}\right), \tag{A3}$$

which is the effective mode length characterizing EM-field confinement in the z direction.

APPENDIX B: BLOCH EQUATIONS IN THE INTERACTION PICTURE

The Bloch equations in the interaction picture are given by

$$i\frac{\partial}{\partial t}\sigma_{11} - i\Gamma_{13}\sigma_{33} - i\Gamma_{14}\sigma_{44} + \zeta^*(z)\Omega_p^*\sigma_{31} - \zeta(z)\Omega_p\sigma_{31}^* = 0, \tag{B1a}$$

$$i\frac{\partial}{\partial t}\sigma_{22} - i\Gamma_{23}\sigma_{33} - i\Gamma_{24}\sigma_{44} + \zeta^*(z)\Omega_s^*\sigma_{32} - \zeta(z)\Omega_s\sigma_{32}^* + \zeta^*(z)\Omega_c^*\sigma_{42} - \zeta(z)\Omega_c\sigma_{42}^* = 0, \tag{B1b}$$

$$i\left(\frac{\partial}{\partial t} + \Gamma_3\right)\sigma_{33} + \zeta(z)\Omega_s\sigma_{32}^* + \zeta(z)\Omega_p\sigma_{31}^* - \zeta^*(z)\Omega_s^*\sigma_{32} - \zeta^*(z)\Omega_p^*\sigma_{31} = 0, \tag{B1c}$$

$$i\left(\frac{\partial}{\partial t} + \Gamma_4\right)\sigma_{44} + \zeta(z)\Omega_c\sigma_{42}^* - \zeta^*(z)\Omega_c^*\sigma_{42} = 0, \tag{B1d}$$

$$\left(i\frac{\partial}{\partial t} + d_{21}\right)\sigma_{21} + \zeta^*(z)\Omega_c^*\sigma_{41} + \zeta^*(z)\Omega_s^*\sigma_{31} - \zeta(z)\Omega_p\sigma_{32}^* = 0, \tag{B1e}$$

$$\left(i\frac{\partial}{\partial t} + d_{31}\right)\sigma_{31} + \zeta(z)\Omega_p(\sigma_{11} - \sigma_{33}) + \zeta(z)\Omega_s\sigma_{21} = 0, \tag{B1f}$$

$$\left(i\frac{\partial}{\partial t} + d_{32}\right)\sigma_{32} + \zeta(z)\Omega_p\sigma_{21}^* + \zeta(z)\Omega_s(\sigma_{22} - \sigma_{33}) - \zeta(z)\Omega_c\sigma_{43}^* = 0, \tag{B1g}$$

$$\left(i\frac{\partial}{\partial t}+d_{41}\right)\sigma_{41}+\zeta(z)\Omega_c\sigma_{21}-\zeta(z)\Omega_p\sigma_{43}=0, \tag{B1h}$$

$$\left(i\frac{\partial}{\partial t}+d_{42}\right)\sigma_{42}+\zeta(z)\Omega_c(\sigma_{22}-\sigma_{44})-\zeta(z)\Omega_s\sigma_{43}=0, \tag{B1i}$$

$$\left(i\frac{\partial}{\partial t}+d_{43}\right)\sigma_{43}+\zeta(z)\Omega_c\sigma_{32}^{*}-\zeta^{*}(z)\Omega_p^{*}\sigma_{41}-\zeta^{*}(z)\Omega_s^{*}\sigma_{42}=0, \tag{B1j}$$

where $d_{21}=-(k_p-k_s)v+\Delta_2-\Delta_1+i\gamma_{21}$, $d_{31}=-k_pv+\Delta_3-\Delta_1+i\gamma_{31}$, $d_{32}=-k_sv+\Delta_3-\Delta_2+i\gamma_{32}$, $d_{41}=-(k_p+k_c-k_s)v+\Delta_4-\Delta_1+i\gamma_{41}$, $d_{42}=-k_cv+\Delta_4-\Delta_2+i\gamma_{42}$, and $d_{43}=-(k_c-k_s)v+\Delta_4-\Delta_3+i\gamma_{43}$, with $\gamma_{jl}=(\Gamma_j+\Gamma_l)/2+\gamma_{jl}^{\rm col}$ $(j,l=1\text{–}4)$. Here Γ_j and Γ_l are the total decay rates of the population out of levels $|j\rangle$ and $|l\rangle$, respectively, defined by $\Gamma_i=\sum_{j\neq i}\Gamma_{ji}$. The quantity $\gamma_{ij}^{\rm col}$ is the proper dephasing rate.

APPENDIX C: EXPRESSIONS OF THE COEFFICIENTS OF THE LINEAR SOLUTION

The expressions of the coefficients of the linear solution are given by

$$a_{32}^{(1)}=\frac{B\left(\sigma_{33}^{(0)}-\sigma_{22}^{(0)}\right)-[D_p+|\zeta(z)\Omega_c|^2]\zeta(z)\Omega_p\sigma_{31}^{*(0)}-[D_c+|\zeta(z)\Omega_p|^2]\zeta(z)\Omega_c\sigma_{42}^{*(0)}}{(\omega+d_{32})B-|\zeta(z)\Omega_p|^2[D_p+|\zeta(z)\Omega_c|^2]|\zeta(z)\Omega_c|^2[D_c+|\zeta(z)\Omega_p|^2]},$$

$$a_{21}^{*(1)}=\frac{1}{B}\left\{D_p\sigma_{31}^{*(0)}+\Omega_c\Omega_p^{*}|\zeta(z)|^2\sigma_{42}^{*(0)}-[D_p+|\zeta(z)\Omega_c|^2]\zeta^{*}(z)\Omega_p^{*}\sigma_{32}^{(1)}\right\},$$

$$a_{43}^{*(1)}=\frac{1}{B}\left\{[D_c+|\zeta(z)\Omega_p|^2]\zeta^{*}(z)\Omega_c^{*}\sigma_{32}^{(1)}-D_c\sigma_{42}^{*(0)}-\Omega_p\Omega_c^{*}|\zeta(z)|^2\sigma_{31}^{*(0)}\right\},$$

$$a_{41}^{*(1)}=\frac{1}{\omega-d_{41}^{*}}\left[\zeta(z)\Omega_ca_{21}^{*(1)}-\zeta(z)\Omega_pa_{43}^{*(1)}\right].$$

APPENDIX D: EXPRESSIONS OF THE SECOND-ORDER SOLUTION

The expressions of the second-order solution are given by

$$\begin{aligned}\sigma_{11}^{(2)}&=\frac{[2(\Gamma_{23}+\Gamma_{14})\gamma_{42}|\zeta(z)\Omega_c|^2-i\Gamma_{23}A_4]J_1+iA_3\Gamma_{14}J_2+[A_4+2i\gamma_{42}|\zeta(z)\Omega_c|^2]A_3J_3}{-2\Gamma_{23}\gamma_{31}A_4|\zeta(z)\Omega_p|^2-2\gamma_{42}|\zeta(z)\Omega_c|^2[A_3\Gamma_{14}+2i(\Gamma_{13}+\Gamma_{14})\gamma_{31}|\zeta(z)\Omega_p|^2]}|\zeta(z)|^2|F|^2e^{-2\alpha x}\\&\equiv a_{11}^{(2)}|\zeta(z)|^2|F|^2e^{-2\alpha x},\end{aligned} \tag{D1a}$$

$$\sigma_{33}^{(2)}=\frac{2i\gamma_{31}|\zeta(z)\Omega_p|^2a_{11}^{(2)}+J_1}{A_3}|\zeta(z)|^2|F|^2e^{-2\alpha x}\equiv a_{33}^{(2)}|\zeta(z)|^2|F|^2e^{-2\alpha x}, \tag{D1b}$$

$$\sigma_{44}^{(2)}=\frac{i\Gamma_{23}a_{33}^{(2)}+J_3}{i\Gamma_{14}}|\zeta(z)|^2|F|^2e^{-2\alpha x}\equiv a_{44}^{(2)}|\zeta(z)|^2|F|^2e^{-2\alpha x}, \tag{D1c}$$

$$\sigma_{22}^{(2)}=\frac{A_4a_{44}^{(2)}-J_2}{2i\gamma_{42}|\zeta(z)\Omega_c|^2}|\zeta(z)|^2|F|^2e^{-2\alpha x}\equiv a_{22}^{(2)}|\zeta(z)|^2|F|^2e^{-2\alpha x}, \tag{D1d}$$

$$\sigma_{31}^{(2)}=\frac{1}{d_{31}}\left[\zeta(z)\Omega_p\left(a_{33}^{(2)}-a_{11}^{(2)}\right)-a_{21}^{(1)}\right]|\zeta(z)|^2|F|^2e^{-2\alpha x}\equiv a_{31}^{(2)}|\zeta(z)|^2|F|^2e^{-2\alpha x}, \tag{D1e}$$

$$\sigma_{42}^{(2)}=\frac{1}{d_{42}}\left[\zeta(z)\Omega_c\left(a_{44}^{(2)}-a_{22}^{(2)}\right)+a_{43}^{(1)}\right]|\zeta(z)|^2|F|^2e^{-2\alpha x}\equiv a_{42}^{(2)}|\zeta(z)|^2|F|^2e^{-2\alpha x}, \tag{D1f}$$

with $A_3=i[\Gamma_3|d_{31}|^2+2\gamma_{31}|\zeta(z)\Omega_p|^2]$, $A_4=i[\Gamma_4|d_{42}|^2+2\gamma_{42}|\zeta(z)\Omega_c|^2]$, $J_1=|d_{31}|^2a_{32}^{(1)}+d_{31}\zeta(z)\Omega_pa_{21}^{*(1)}-\text{c.c.}$, $J_2=d_{42}^{*}\zeta^{*}(z)\Omega_c^{*}a_{43}^{(1)}-\text{c.c.}$, and $J_3=a_{32}^{(1)}-\text{c.c.}$ The other matrix elements of the second-order solution are

$$\begin{pmatrix}\sigma_{21}^{*(2)}\\ \sigma_{32}^{(2)}\\ \sigma_{41}^{*(2)}\\ \sigma_{43}^{*(2)}\end{pmatrix}=\begin{pmatrix}\omega-d_{21}^{*} & \zeta^{*}(z)\Omega_p^{*} & -\zeta(z)\Omega_c & 0\\ \zeta(z)\Omega_p & \omega+d_{32} & 0 & -\zeta(z)\Omega_c\\ -\zeta(z)\Omega_c & 0 & \omega-d_{41}^{*} & \zeta^{*}(z)\Omega_p^{*}\\ 0 & -\zeta^{*}(z)\Omega_c^{*} & \zeta(z)\Omega_p & \omega-d_{43}^{*}\end{pmatrix}^{-1}\begin{pmatrix}-i\frac{\partial}{\partial t_1}\sigma_{21}^{*(1)}\\ -i\frac{\partial}{\partial t_1}\sigma_{32}^{(1)}\\ -i\frac{\partial}{\partial t_1}\sigma_{41}^{*(1)}\\ -i\frac{\partial}{\partial t_1}\sigma_{43}^{*(1)}\end{pmatrix}. \tag{D2}$$

When the half Rabi frequency of the control field is spatially modulated with $\Omega_c = \Omega_c^{(0)}[1 + \epsilon^2\Omega_c^{(2)}(y)]$, the expressions of the second-order solution are the same as Eqs. (D1) and (D2), but with $J_2 = d_{42}^*\zeta^*(z)\Omega_c^{(0)*}[a_{43}^{(1)} + \Omega_c^{(2)}(y)(\sigma_{44}^{(0)} - \sigma_{22}^{(0)})/|F|^2e^{-2\alpha x}] -$ c.c. and with Ω_c replaced by $\Omega_c^{(0)}$.

[1] S. A. Maier, *Plasmonics: Fundamentals and Applications* (Springer, Berlin, 2007).

[2] D. Sarid and W. Challener, *Modern Introduction to Surface Plasmons: Theory, Mathematica Modeling, and Applications* (Cambridge University Press, Cambridge, 2010).

[3] M. I. Stockman, J. Opt. **12**, 024004 (2010), and references therein.

[4] P. Berini and I. De Leon, Nat. Photon. **6**, 16 (2012), and references therein.

[5] J. B. Khurgin and G. Sun, Nat. Photon. **8**, 468 (2014).

[6] D. J. Bergman and M. I. Stockman, Phys. Rev. Lett. **90**, 027402 (2003).

[7] D. E. Chang, A. S. Sørensen, P. R. Hemmer, and M. D. Lukin, Phys. Rev. Lett. **97**, 053002 (2006).

[8] A. V. Akimov *et al.*, Nature (London) **450**, 402 (2007).

[9] I. De Leon and P. Berini, Phys. Rew. B **78**, 161401(R) (2008).

[10] M. A. Noginov, G. Zhu, M. Mayy, B. A. Ritzo, N. Noginova, and V. A. Podolskiy, Phys. Rev. Lett. **101**, 226806 (2008).

[11] R. F. Oulton *et al.*, Nature (London) **461**, 629 (2009).

[12] D. Dzsotjan, A. S. Sørensen, and M. Fleischhauer, Phys. Rev. B **82**, 075427 (2010).

[13] P. M. Bolger *et al.*, Opt. Lett. **35**, 1197 (2010).

[14] K. E. Dorfman, P. K. Jha, D. V. Voronine, P. Genevet, F. Capasso, and M. O. Scully, Phys. Rev. Lett. **111**, 043601 (2013).

[15] C. J. Zhu *et al.*, Appl. Phys. Lett. **104**, 203108 (2014).

[16] A. Kamli, S. A. Moiseev, and B. C. Sanders, Phys. Rev. Lett. **101**, 263601 (2008).

[17] S. A. Moiseev, A. A. Kamli, and B. C. Sanders, Phys. Rev. A **81**, 033839 (2010).

[18] M. Siomau, A. A. Kamli, S. A. Moiseev, and B. C. Sanders, Phys. Rev. A **85**, 050303(R) (2012).

[19] For ARG, see, e.g., L. Deng and M. G. Payne, Phys. Rev. Lett. **98**, 253902 (2007).

[20] For superluminal (or fast) light (i.e., the light with group velocity large than c and even negative) and its applications, see R. W. Boyd and D. J. Gauthier, Science **326**, 1074 (2009).

[21] The frequency and wave number of the signal field are given by $\omega_s + \omega$ and $k_s + K(\omega)$, respectively. Thus ω is the frequency deviation ($\omega = 0$ corresponds to the center frequency) of the signal field.

[22] G. Huang, L. Deng, and M. G. Payne, Phys. Rev. E **72**, 016617 (2005).

[23] Y. Liu, G. Bartal, D. A. Genov, and X. Zhang, Phys. Rev. Lett. **99**, 153901 (2007).

[24] A. Marini and D. V. Skryabin, Phys. Rev. A **81**, 033850 (2010).

[25] A. Marini, D. V. Skryabin, and B. Malomed, Opt. Express **19**, 6616 (2011).

[26] E. Feigenbaum and M. Orenstein, Opt. Lett. **32**, 674 (2007).

[27] A. R. Davoyan, I. V. Shadrivov, and Y. S. Kivshar, Opt. Express **17**, 21732 (2009).

[28] C. Tan and G. Huang, Phys. Rev. A **89**, 033860 (2014).

[29] J. N. Gollub, D. R. Smith, D. C. Vier, T. Perram, and J. J. Mock, Phys. Rev. B **71**, 195402 (2005).

[30] V. M. Shalaev, Nat. Photon. **1**, 41 (2007).

[31] G. Dolling, M. Wegener, C. M. Soukoulis, and S. Linden, Opt. Lett. **32**, 53 (2007).